



This is the accepted manuscript made available via CHORUS, the article has been published as:

Nanoplasmonic Lattices for Ultracold Atoms

M. Gullans, T. G. Tiecke, D. E. Chang, J. Feist, J. D. Thompson, J. I. Cirac, P. Zoller, and M. D. Lukin

Phys. Rev. Lett. **109**, 235309 — Published 6 December 2012

DOI: [10.1103/PhysRevLett.109.235309](https://doi.org/10.1103/PhysRevLett.109.235309)

Nanoplasmonic Lattices for Ultracold Atoms

M. Gullans,¹ T. Tiecke,^{1,2} D. E. Chang,³ J. Feist,¹ J. D. Thompson,¹ J. I. Cirac,⁴ P. Zoller,⁵ and M. D. Lukin¹

¹*Department of Physics, Harvard University, Cambridge, MA 02138, USA*

²*MIT-Harvard Center for Ultracold Atoms, and Research Laboratory of Electronics, MIT, Cambridge, Massachusetts 02139, USA*

³*ICFO-Institut de Ciències Fotoniques, Mediterranean Technology Park, 08860 Castelldefels (Barcelona), Spain*

⁴*Max-Planck-Institut für Quantenoptik, Hans-Kopfermann-Str. 1, D-85748 Garching, Germany*

⁵*Institute for Theoretical Physics, University of Innsbruck, 6020 Innsbruck, Austria*

(Dated: November 27, 2012)

We propose to use sub-wavelength confinement of light associated with the near field of plasmonic systems to create nanoscale optical lattices for ultracold atoms. Our approach combines the unique coherence properties of isolated atoms with the sub-wavelength manipulation and strong light-matter interaction associated with nano-plasmonic systems. It allows one to considerably increase the energy scales in the realization of Hubbard models and to engineer effective long-range interactions in coherent and dissipative many-body dynamics. Realistic imperfections and potential applications are discussed.

PACS numbers: 37.10.Gh, 42.50.-p, 73.20.Mf, 78.67.Bf

Coherent optical fields provide a powerful tool for manipulating ultracold atoms [1, 2]. However, diffraction sets a fundamental limit for the length-scale of such manipulations, given by the wavelength of light [3]. In particular, the large period of optical lattices determines the energy scale of the associated many-body atomic states [4–7]. The resulting scaling can be best understood by noting that in the first Bloch band the maximum atomic momentum $\sim 1/\ell$, where ℓ is the lattice spacing. This sets the maximum kinetic energy to $\hbar^2/m\ell^2$ [8]. For conventional optical lattices the lattice spacing is set by half the wavelength of the trapping light ~ 500 nm; this yields corresponding tunneling rates of up to a few tens of kHz. Additionally, for atoms in their electronic ground states interactions are restricted to short range.

Recent experimental [9] and theoretical [10, 11] work has demonstrated that integrating plasmonic systems with cold atoms represents a promising approach to achieving subwavelength control of atoms. In particular, the experiments of Ref. [9] showed that ultracold atoms can be used to probe the near fields of plasmonic structures, paving the way to eventually trap atoms above such structures. In this Letter we propose and analyze a novel approach to the realization of high-density optical lattices using the optical potential formed from the near field scattering of light by an array of plasmonic nanoparticles. By bringing atom trapping into the subwavelength and nanoscale regime we show that the intrinsic scales of tunneling and onsite interaction for the Hubbard model can be increased by several orders of magnitude compared to conventional optical lattices. In addition, sub-wavelength confinement of the atoms results in strong radiative interactions with the plasmonic modes of the nanoparticles [12]. The coupled atom-plasmon system can be considered as a scalable cavity array that results in strong, long range spin-spin interactions between the atoms with both dissipative and coherent contributions

[13, 14]. Such a system can be used for entanglement of remote atoms as well as for novel realizations of coherent and dissipative many-body systems.

To illustrate our approach we first consider a single metallic nanosphere in vacuum illuminated by a plane wave. For spheres small compared to a wavelength the dominant contribution to the scattered field is the dipole term, where the induced dipole moment is given by $\mathbf{p} = \alpha(\omega)\mathbf{E}_0$ with

$$\alpha(\omega) = 4\pi\epsilon_0 a^3 \frac{\epsilon(\omega) - 1}{\epsilon(\omega) + 2} \quad (1)$$

where a is the radius of the sphere and ϵ is the permittivity [15]. The total electric field is

$$\mathbf{E} = \mathbf{E}_0 + \frac{\alpha(\omega)}{4\pi\epsilon_0} \frac{3(\hat{r} \cdot \mathbf{E}_0)\hat{r} - \mathbf{E}_0}{r^3} \quad (2)$$

Near $\epsilon(\omega_{sp}) = -2$ there is a plasmon resonance and the scattered field can be engineered to create an optical dipole trap as depicted in Fig. 1b. Specifically, when the applied field is linearly polarized on the blue side of the plasmon resonance then the induced dipole will be $\sim \pi$ out phase with the incident field, leading to two intensity minima along the polarization direction at the positions $z_T^2 = \pm 2a^3\omega_{sp}^2/(\omega^2 - \omega_{sp}^2)$, where we took a Lorentzian polarizability near the resonance $\alpha(\omega) = 4\pi\epsilon_0 a^3 \omega_{sp}^2/(\omega_{sp}^2 - \omega^2 - i\omega\kappa)$, with κ the linewidth. For red detuned, circularly polarized light, there will be two minima along the propagation axis. An atom can be trapped in these intensity minima via optical dipole forces [2]. The trapping potential is given by $\hbar\Omega^2/\delta$, where $\Omega = \boldsymbol{\mu}_0 \cdot \mathbf{E}/\hbar$ is the Rabi frequency, $\boldsymbol{\mu}_0$ is the atomic dipole moment, and $\delta = \omega_a - \omega$ is the detuning between the atom and laser. Expanding near the trap minima gives the trapping frequency $\omega_T^2 = 9 \frac{\hbar\Omega_0^2}{\delta m z_T^2} \text{Re}(\alpha)^2/|\alpha|^2 \sim \hbar\Omega_0^2/\delta m a^2$.

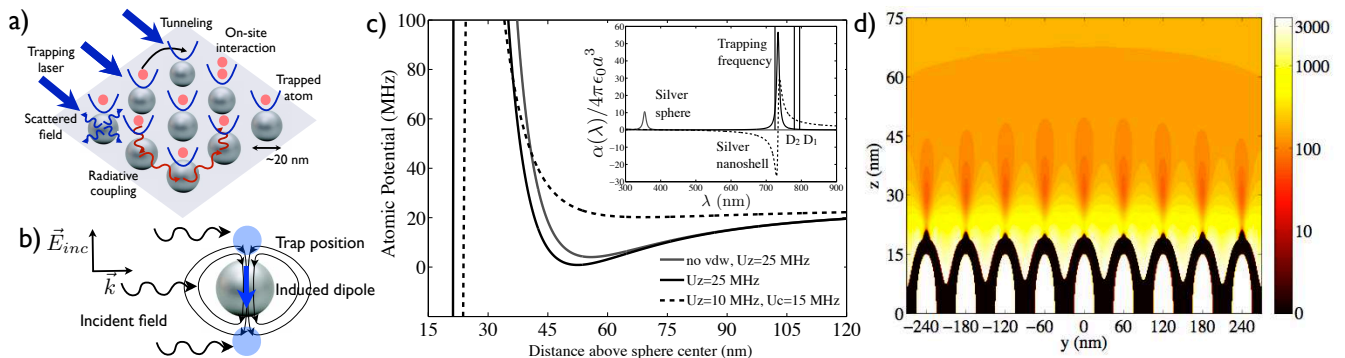


FIG. 1: a) Illustration of the relevant physics in the plasmonic lattice. b) Illustration of how to engineer a blue-detuned optical dipole trap by driving on the blue side of the plasmon resonance. c) Atomic potential for Rb including van der Waals (vdw) for trapping above a single silver nanoshell. Dotted line shows how to weaken the trap by applying circularly polarized light perpendicular to the trapping light. (Inset) Real (dashed) and imaginary (solid) part of the dipole polarizability for a sphere and the nanoshell with a 15 nm radius and 13.85 nm SiO₂ core. d) y - z contours of atomic potential in MHz for a line of nine spheres in the center of a 45x45 square lattice with a 60 nm lattice spacing, black regions are where the potential is negative due to vdw, spheres are shown in white. The nanoshells are silver with a 15 nm radius and 13.65 nm SiO₂ core, the trapping light is red detuned (704 nm) wrt to the plasmon resonance (682 nm) and applied from above with rotating x - y polarized light.

The trap depth can be controlled by applying a second field with the opposite polarization, as illustrated in Fig. 1c. Using this method, the atoms can be loaded into the near field traps by starting with a cold, dense gas of atoms in a large trap and then adiabatically turning on the near field traps.

We now address several practical considerations. First, for alkali atoms there is a large disparity between the natural plasmon resonance and the atomic trapping transitions. For a solid silver sphere the plasmon resonance occurs near 350 nm [16], compared to 780 nm for the D2 line in Rb. However, the plasmon resonance is easily tuned by changing the geometry. Adding an inert core, such as SiO₂, will shift the plasmon resonance into the red [17], as illustrated in the inset to Fig. 1c.

There will also be significant surface interactions. Van der Waals (vdw) forces can be overcome with modest laser power because of the sphere's plasmonic enhancement [10, 11]. There are two dominant sources of heating and decoherence arising from incoherent transitions induced by the trapping laser or thermal magnetic field noise in the nanoparticle. The first effect scales as $\gamma\Omega^2/\delta^2$, where γ is the atomic linewidth, and is suppressed at large detuning. To estimate the effect of magnetic field noise we approximate the nanoshell as a current loop of radius and height a , thickness t , and resistivity ρ . Then the incoherent transition rate between hyperfine states is $\sim (g_F\mu_0\mu_B)^2 k_B T (a^4 t / r^5) / \hbar^2 \rho r$, where r is the distance of the atom to the sphere center, g_F is the hyperfine g -factor, μ_B is the Bohr magneton, and T is the temperature [18].

Figures 1cd show the atomic trapping potential for a single sphere and an array, respectively. We numerically

obtained the trapping potential in Fig. 1c using Mie theory and the vdw potential was obtained using the methods in Ref. [20]. To solve for the trapping potential in the array in Fig. 1d we approximated the scattered field from each nanoshell by a dipole and solved for the total field self-consistently. Using the parameters in Fig. 1c for trapping ⁸⁷Rb above a silver nanoshell at room temperature with $\Omega_0 = 25$ GHz (corresponding to $\sim 10^8 I_{\text{sat}}$, where $I_{\text{sat}} \approx 1.7$ mW/cm²) and $\delta = 25$ THz, we estimate a trap depth of ~ 25 MHz and a trapping frequency of ~ 5 MHz. Both the magnetic field noise and laser detuning limit the decoherence rate to ~ 10 Hz and the heating rate to ~ 1 Hz, meaning that the atom can be trapped for ~ 1 second.

The controlled patterning of arrays of metallic nanoparticles can be done lithographically in a top-down approach or through the controlled self-assembly of metallic nanoparticles in a bottom-up approach [21–24]. In any nanofabricated system one must contend with disorder; the relevant disorder in this system occurs in the particle positioning and particle formation. In lithographic approaches one can control the particle formation at the level of 1-2 nm [22]. In bottom-up, self-assembly approaches it is possible to create large regions of well ordered crystal with a finite density of point and line defects, much like a conventional solid [24]. Due to the local nature of the traps the disorder in the particle positioning will not affect the trapping. Errors in the particle formation can influence the trap by shifting the plasmon resonance and the field enhancement of each particle. To achieve consistent traps the fractional error in the plasmon resonance should be smaller than its inverse quality factor $Q = \omega_{sp}/\kappa$, which for silver(gold) nanospheres

goes up to 80(20) [16, 25]. Currently, metallic nanoshells can be made with a fractional error in the radius of less than 5%, which is comparable to the inverse of Q [26].

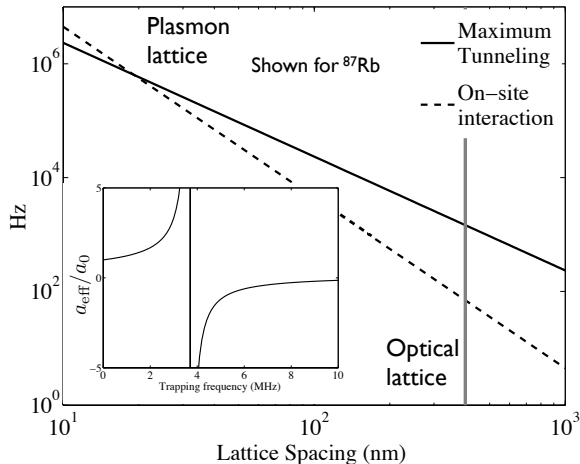


FIG. 2: Shows the scaling of the maximum tunneling in the lowest band, and the corresponding on-site interaction. Calculated using the Wannier functions for a sinusoidal potential. (Inset) Energy dependent scattering length for two ^{87}Rb atoms on a single site as a function of the trap frequency.

As a first example application of this system we consider a realization of the single-band Hubbard model in the novel regime of large atomic density [1]. As an example, Fig. 1d shows that a well defined lattice potential can be achieved with a period of 60 nm, which is within current fabrication limits. Figure 2a illustrates the scaling for the maximum tunneling in the lowest band and the corresponding on-site interaction U_0 . [8]. In the supplementary material we show that the tunneling rate can also be tuned through appropriate polarization control [19].

These nanoscale traps reach a regime of atomic confinement where the ground state uncertainty becomes comparable to the free space scattering length. For two atoms in a 3D isotropic trap the two-body scattering problem can be solved exactly, leading to an effective scattering length $a_{\text{eff}}(\omega_T)$ which depends on the confinement energy [27, 28]. The inset of Figure 2 shows that a resonance emerges in the effective scattering length as a function of trap frequency [19].

Disorder in the lattice will also effect the Hubbard model. The dominant effect arises from shifts in the local atomic potential at each sphere as the plasmonic enhancement factor changes from site to site. From Eq. 2 one can show that the rms of the disorder potential is given by $U_{\text{dis}} \approx \frac{\Omega^2}{2\delta} (z_T^9/a^9 Q^2)\eta/\omega_{sp}$, where η is the rms error in the plasmon resonance. If we take $\eta/\omega_{sp} \sim 5\%$, then for a wide range of parameters, including those in

Fig. 1d, we find that U_{dis} can be made smaller than, or comparable to, the maximum tunneling. In addition, since the disorder is static one can reduce it using the techniques described in Ref. [29]. The effect of disorder on the single-particle physics is well understood [30]; moreover, the interplay between interactions and disorder in the Hubbard model, as studied in Ref. [31–34], is an interesting new regime which can be explored in the present system.

We now consider long range interactions within the plasmonic lattice, associated with the strong radiative coupling between the atoms and spheres [35]. This can be viewed as a strongly coupled cavity QED system. The coupling between the atoms and the near field of the sphere is given by $g \sim \mu_0 d_0 / \epsilon_0 r^3$ where $d_0 = \sqrt{\hbar \omega_{sp} \alpha(0)} / 2$ is the quantized dipole moment of the sphere [36]. Since the plasmons are overdamped the relevant coupling is given by the Purcell factor $P = g^2 / \kappa \gamma$. The plasmon linewidth κ has contributions from radiative and ohmic losses. The radiative damping rate is $k^3 d_0^2 / 3\pi \epsilon_0 \hbar \sim k^3 a^3 \omega_{sp}$. Large spheres are radiatively broadened and, in this case, $P \sim (kr)^{-6}$, while for small spheres $P \sim Qa^3 / k^3 r^6$. In both limits, when $r \ll \lambda / 2\pi \sim 100$ nm the atoms enter the strong coupling regime $P \gg 1$, see Figure 3a [37].

For a lattice of nanospheres, intersphere coupling is also present and leads to delocalized plasmon modes in the lattice [38, 39]. We calculate the interaction of two atoms through these modes in a 1D chain of nanospheres. For each sphere in the chain we can write the self-consistent equation for their dipole moments as [40]

$$\mathbf{p}_n = \alpha(\omega)(\mathbf{E}_n + \mathbf{N}_{nm}\mathbf{p}_m) \quad (3)$$

where \mathbf{p}_n is the induced dipole moment of the n th nanoparticle, \mathbf{E}_n is the incident field, and \mathbf{N}_{nm} is the 3×3 matrix that gives the dipole field at site n due to the dipole at site m . In 1D two sets of transverse modes where the dipoles are oriented perpendicular to the chain and one set of longitudinal modes for parallel orientation. Defining $\tilde{\mathbf{p}}_q$ to be the q th eigenvector of \mathbf{N}_{nm} with eigenvalue D_q , then the effective polarizability of the q th mode is $\alpha_q^{-1} = \alpha^{-1} - D_q$, i.e. $\tilde{\mathbf{p}}_q = \alpha_q \tilde{\mathbf{E}}_q$. For a Lorentzian polarizability the real part of D_q gives the shift in the resonance frequency of the q th mode and the imaginary part gives the change in the linewidth. \mathbf{N}_{nm} is diagonalized by Fourier transform and if we neglect all but nearest neighbor terms $D_q = 2N_{01}^r \cos q - ik^3 / 6\pi \epsilon_0$, where $N_{01}^r = \text{Re}(N_{01})$.

Let us consider atoms trapped above the 1D array of spheres. The plasmonic modes can be adiabatically eliminated using standard methods in quantum optics [41]. For two-level atoms polarized parallel to the 1D chain

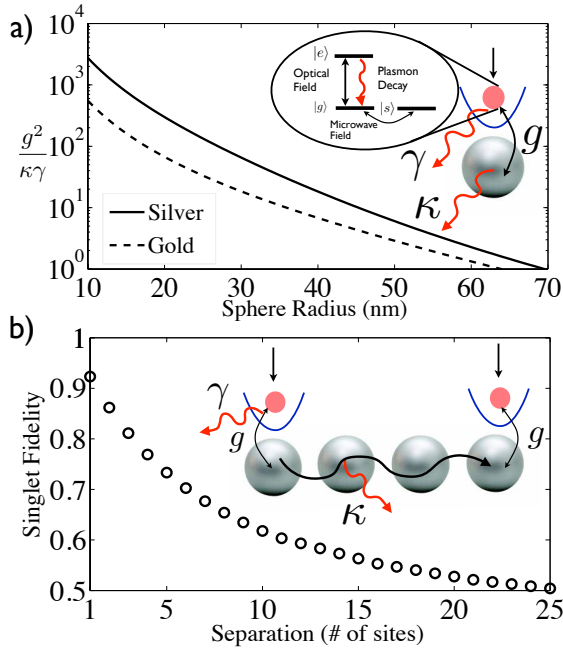


FIG. 3: a) Shows the cavity QED figure of merit $g^2/\kappa\gamma$ with changing system size assuming the atom is trapped at a distance of twice the sphere radius. We show the scaling for both silver and gold nanoshells with a Q of 80 and 20, respectively. (Inset) Single atom trapped above a nanosphere acts as cavity QED system with atomic and cavity losses γ and κ , respectively, and a coherent coupling g . b) Fidelity for generating a ground state singlet state between two atoms on the lattice with their separation after optimization. The entanglement is generated through interaction with the collective plasmon modes, where we took the metal losses of bulk silver. (Inset) Scalable cavity QED array of atoms and plasmons.

the atomic density matrix evolution is

$$\dot{\rho} = -\frac{i\omega_{at}}{2} \sum_n [\sigma_n^z, \rho] - \frac{i}{2} \sum_{nm} \delta\omega_{nm} [\sigma_n^+ \sigma_m^-, \rho] - \frac{1}{2} \sum_{n,m} \gamma_{nm} (\{\sigma_n^+ \sigma_m^-, \rho\} - 2\sigma_m^- \rho \sigma_n^+) \quad (4)$$

$$\delta\omega_{nm} = -\frac{3\ell^3}{8k^3 z^6} \Gamma_0 \operatorname{Re} \left(\frac{i e^{iq_r^* |n-m|}}{\sin q^*} \right) e^{-q_i^* |n-m|} \quad (5)$$

$$\gamma_{nm} = \frac{3\ell^3}{8k^3 z^6} \Gamma_0 \operatorname{Im} \left(\frac{i e^{iq_r^* |n-m|}}{\sin q^*} \right) e^{-q_i^* |n-m|} \quad (6)$$

where z is the position of the atoms above the sphere and $q^* = q_r^* + i q_i^*$ is the resonant wavevector such that $\alpha_{q^*}^{-1}(\omega_a) = 0$. The first line in Eq. 4 describes the coherent evolution and the second line describes the collective dissipation. Here we have neglected the contribution to the interaction from free-space radiative modes.

The coherent and dissipative contributions to Eq. 4 are equally strong when the atom and plasmon are near resonant. Working far off resonance, however, results in purely coherent dynamics, which can be used to imple-

ment long-range interacting spin models including frustration [42, 43]. Alternatively, the collective dissipative dynamics can be used to prepare correlated atomic states [44]. As an example, we now show how to directly prepare a ground state singlet between two atoms separated by large distances on the lattice. We take two ground states $|g\rangle$ and $|s\rangle$ and an excited state $|e\rangle$ which is coupled to $|g\rangle$ via an external field and only decays via the plasmons back to $|g\rangle$ (see inset to Fig. 3a). An external microwave field mixes the two ground states. To prepare the singlet state $|S\rangle = |gs\rangle - |sg\rangle$ we use a similar approach to Ref. [45] whereby the singlet state is engineered to be the steady state of a driven, dissipative evolution. We take a separation n such that $\cos q_r^* n = 1$ and

$$\dot{\rho} = -\gamma_{0n} \mathcal{D}[\sigma_1^{ge} + \sigma_2^{ge}] \rho - \delta\gamma_n (\mathcal{D}[\sigma_1^{ge}] + \mathcal{D}[\sigma_2^{ge}]) \rho \quad (7)$$

where $\mathcal{D}[c]\rho = 1/2\{c^\dagger c, \rho\} - c\rho c^\dagger$ and $\delta\gamma_n = \gamma_{00} - \gamma_{n0} \sim \gamma_{00} (\ell^3/a^3)n/Q$ for $n \ll Q$. The dynamics can be mapped to a cavity QED system by identifying γ_{0n} with the collective decay g^2/κ and $\delta\gamma_n$ with the free space decay γ . The two excited states $|eg\rangle$ and $|ge\rangle$ split into a superradiant state $|eg\rangle + |ge\rangle$ and a subradiant state $|eg\rangle - |ge\rangle$ with decay rates $2\gamma_{0n} + \delta\gamma_n$ and $\delta\gamma_n$, respectively.

The singlet preparation proceeds as follows. First, we selectively excite the subradiant transition $|gg\rangle$ to $|ge\rangle - |eg\rangle$ by driving with a weak external laser field $\Omega \sim \delta\gamma_n \ll \gamma_{00}$, which we take to have a π phase difference on the two atoms. Second, in order to make the singlet state a unique steady state, we apply a global microwave field to mix the triplet ground states without affecting the singlet state. In the resulting dynamics, the pumping rate into the singlet state is $\Omega^2/\delta\gamma_n$, while the pumping rate back into the triplets is Ω^2/γ_{00} [19]. The steady state of this process gives the singlet state with fidelity $F = \langle S|\rho|S\rangle \sim 1 - 1/P'$ where $P' = \gamma_{00}/\delta\gamma_n$. Fig. 3b shows the fidelity for two atoms with variable separation obtained from numerical simulation of Eq. 4.

To measure the correlations in this system, an all optical approach could be realized by making the nanoparticle array in the near field of a solid immersion lens (SIL), which enhances the resolution beyond the diffraction limit by a factor of n , the index of refraction of the SIL [46]. Combining a SIL with e.g. super resolution microscopy techniques would allow one to reach the requisite resolution of ~ 50 nm at optical wavelengths [47].

Our analysis shows that combining cold atom techniques with nanoscale plasmonics reaches new regimes in controlling both the collective motion of atoms and atom-photon interactions. Combining excellent quantum control of isolated atoms with nanoscale localization, may open up exciting new possibilities for quantum control of ultracold atoms.

This work was supported by the Harvard-MIT CUA, NSF, the Physics Frontier Center, EU project AQUATE, the ARO, DARPA OLE program, and Stanford AFOSR MURI #FA9550-12-1-0024.

-
- [1] I. Bloch, J. Dalibard, and S. Nascimbene, *Nat. Phys.* 8, 267 (2012)
- [2] R. Grimm, M. Weidemller, Y. B. Ovchinnikov, *Adv. Atom., Mol. and Opt. Phys.* Vol. 42, 95 (2000)
- [3] E. Hecht, *Optics*, 3rd Ed., (Addison-Wesley, 1998)
- [4] I. Buluta and F. Nori, *Science* 326, 108 (2009)
- [5] W. Yi, A. J. Daley, G. Pupillo, and P. Zoller, *New Journal of Physics* 10, 073015 (2008); A. Gorshkov, L. Jiang, M. Greiner, P. Zoller, and M. D. Lukin, *Phys. Rev. Lett.* 100, 093005 (2008).
- [6] V.Y.F. Leung, A. Tauschinsky, N.J. van Druten, and R.J.C. Spreeuw, arXiv 1104.3067 (2012).
- [7] M. Lewenstein, A. Sanpera, and V. Ahufinger, *Ultracold Atoms in Optical Lattices: Simulating Quantum Many-Body Systems* (Oxford University Press, 2012)
- [8] D. Jaksch, C. Bruder, J. I. Cirac, C. W. Gardiner, and P. Zoller, *Phys. Rev. Lett.* 81, 3108 (1998).
- [9] C. Stehle, H. Bender, C. Zimmermann, D. Kern, M. Fleischer, and S. Slama, *Nat. Phot.* 5, 494 (2011).
- [10] B. Murphy and L. V. Hau, *Phys. Rev. Lett.* 102, 033003 (2009);
- [11] D. E. Chang, J. D. Thompson, H. Park, V. Vuletić, A. S. Zibrov, P. Zoller, and M. D. Lukin, *Phys. Rev. Lett.* 103, 123004 (2009).
- [12] N. P. de Leon, M. D. Lukin, and H. Park, *IEEE J. Sel. Topics Quantum Electronics* 18, 1781 (2012).
- [13] J. I. Cirac, P. Zoller, H. J. Kimble, and H. Mabuchi, *Phys. Rev. Lett.* 78, 3221 (1997).
- [14] H.J. Kimble, *Nature* 453, 1023 (2008).
- [15] J.D. Jackson, *Classical Electrodynamics* 3rd Edition, Ch. 10 (John Wiley & Sons, New York, NY, 1999).
- [16] P. B. Johnson and R. W. Christy, *Phys. Rev. B* 6, 4370 (1972); V. P. Drachev, et. al., *Opt. Express* 16, 1186 (2008).
- [17] C. F. Bohren and D. R. Huffman, *Absorption and Scattering of Light by Small Particles*, Ch. 5 (John Wiley & Sons, New York, NY, 1983)
- [18] C. Henkel, S. Potting, and M. Wilkens, *Appl. Phys. B* 69, 379 (1999).
- [19] See supplementary information.
- [20] M. T. H. Reid, A. W. Rodriguez, J. White, and S. G. Johnson, *Phys. Rev. Lett.* 103, 040401 (2009).
- [21] P. Nagpal, N. C. Lindquist, S.-H. Oh, and D. J. Norris, *Science* 325, 594 (2009)
- [22] N. C. Lindquist, P. Nagpal, K. M. McPeak, D. J. Norris, and S.-H. Oh, *Rep. Prog. Phys.* 75, 036501 (2012).
- [23] J. A. Fan, C. Wu, K. Bao, J. Bao, R. Bardhan, N. J. Halas, V N. Manoharan, P. Nordlander, G. Shvets, and F. Capasso, *Science* 328, 1135 (2010)
- [24] M. Grzelczak, J. Vermant, E. M. Furst, and L. M. Liz-Marzan, *ACS Nano* 4, 3591 (2010).
- [25] G. V. Hartland, *Chem. Rev.* 111, 3858 (2011).
- [26] M. Rycenga, C. M. Cobley, J. Zeng, W. Li, C. H. Moran, Q. Zhang, D. Qin, and Y. Xia, *Chem. Rev.* 111, 3669 (2011); M. R. Jones, K. D. Osberg, R. J. Macfarlane, M. R. Langille, and C. A. Mirkin, *Chem. Rev.* 111, 3736 (2011).
- [27] T. Busch, B.G. Englert, K. Rzazewski, and M. Wilkens, *Foundations of Physics* Volume 28, Number 4, 549-559 (1998).
- [28] E. L. Bolda, E. Tiesinga, and P. S. Julienne, *Phys. Rev. A* 66, 013403 (2002).
- [29] H. Pichler, J. Schachenmayer, J. Simon, P. Zoller, and A. J. Daley, arXiv 1205.6189 (2012).
- [30] A. Lagendijk, B. A. Van Tiggelen, and D. Wiersma, *Phys. Today* 62, 24 (2009).
- [31] D. Belitz, and T. R. Kirkpatrick, *Rev. Mod. Phys.* 66, 261 (1994).
- [32] D. Basko, I. Aleiner, and B. Altshuler, *Ann. Phys. N.Y.* 321, 1126 (2006).
- [33] K. Byczuk, W. Hofstetter, and D. Vollhardt, *Phys. Rev. Lett.* 94, 056404 (2005).
- [34] L. Fallani, J. E. Lye, V. Guarrera, C. Fort, and M. Inguscio, *Phys. Rev. Lett.* 98, 130404 (2007).
- [35] D. A. Genov, R. F. Oulton, G. Bartal, and X. Zhang, *Phys. Rev. B* 83, 245312 (2011).
- [36] P. de Vries, D. V. van Coevorden, and A. Lagendijk, *Rev. Mod. Phys.* 70, 447 (1998).
- [37] There are also multipolar corrections to the Purcell factor, but in the supplementary material we show these scale as $\text{Im}((\epsilon - 1)/(\epsilon + 1))a^5/r^5 \sim 10^{-4}$ for silver.
- [38] M. Quinten, A. Leitner, J.R. Krenn, and F.R. Aussenegg, *Opt. Lett.*, 23, 1331 (1998).
- [39] J. R. Krenn, A. Dereux, J. C. Weeber, E. Bourillot, Y. Lacroute, J. P. Goudonnet, G. Schider, W. Gotschy, A. Leitner, F. R. Aussenegg, and C. Girard, *Phys. Rev. Lett.* 82, 2590 (1999).
- [40] Approximating the spheres as dipoles provides an accurate description of the collective plasmonic modes of nanosphere chains provided $\ell > 3a$: S. Y. Park and D. Stroud, *Phys. Rev. B* 69, 125418 (2004).
- [41] See for example, M. Gross and S. Haroche, *Phys. Rep.* 93, 301 (1982).
- [42] S. Gopalakrishnan, B. L. Lev, and P. M. Goldbart, *Nat. Phys.* 5, 845 (2009); P. Strack and S. Sachdev, *Phys. Rev. Lett.* 107, 277202 (2011).
- [43] J. S. Gardner, M. J. P. Gingras, and J. E. Greedan, *Rev. Mod. Phys.* 82, 53 (2010).
- [44] F. Verstraete, M. M. Wolf, and J. I. Cirac, *Nature Phys.* 5, 633 (2009); S. Diehl, A. Micheli, A. Kantian, B. Kraus, H. P. Bchler, and P. Zoller, *Nature Phys.* 4, 878 (2008).
- [45] M. J. Kastoryano, F. Reiter, and A. S. Sørensen, *Phys. Rev. Lett.* 106, 090502 (2011);
- [46] Q. Wu, G. D. Feke, R. D. Grober, and L. P. Ghislain, *Appl. Phys. Lett.* 75, 4064 (1999).
- [47] B. Huang, M. Bates, and X. Zhuang, *Annual Rev. of Biochem.* 78, 993 (2009).